Korean Journal Of Agricultural Science

pISSN : 2466-2402
eISSN : 2466-2410

ENGINEERING

Prediction of moisture contents in green peppers using hyperspectral imaging based on a polarized lighting system

Mohammad Akbar Faqeerzada[1], Anisur Rahman[1,2], Geonwoo Kim[3,*], Eunsoo Park[1], Rahul Joshi[1], Santosh Lohumi[1], Byoung-Kwan Cho[1,4,*]

[1]Department of Biosystems Machinery Engineering, College of Agriculture and Life Science, Chungnam National University, Daejeon 34134, Korea

[2]Department of Farm Power and Machinery, Bangladesh Agricultural University, Mymensingh-2202, Bangladesh

[3]Environmental Microbial and Food Safety Laboratory, Agricultural Research Service, United States Department of Agriculture, Powder Mill Road, BARC-East, Bldg 303, Beltsville, MD 20705, USA

[4]Department of Smart Agriculture System, College of Agricultural and Life Science, Chungnam National University, Daejeon 34134, Korea

[*]Corresponding authors: Geonwoo.Kim@ars.usda.gov, chobk@cnu.ac.kr

Abstract

In this study, a multivariate analysis model of partial least square regression (PLSR) was developed to predict the moisture content of green peppers using hyperspectral imaging (HSI). In HSI, illumination is essential for high-quality image acquisition and directly affects the analytical performance of the visible near-infrared hyperspectral imaging (VIS/NIR-HSI) system. When green pepper images were acquired using a direct lighting system, the specular reflection from the surface of the objects and their intensities fluctuated with time. The images include artifacts on the surface of the materials, thereby increasing the variability of data and affecting the obtained accuracy by generating false-positive results. Therefore, images without glare on the surface of the green peppers were created using a polarization filter at the front of the camera lens and by exposing the polarizer sheet at the front of the lighting systems simultaneously. The results obtained from the PLSR analysis yielded a high determination coefficient of 0.89 value. The regression coefficients yielded by the best PLSR model were further developed for moisture content mapping in green peppers based on the selected wavelengths. Accordingly, the polarization filter helped achieve an uniform illumination and the removal of gloss and artifact glare from the green pepper images. These results demonstrate that the HSI technique with a polarized lighting system combined with chemometrics can be effectively used for high-throughput prediction of moisture content and image-based visualization.

Key words: green pepper, hyperspectral imaging, moisture content, nondestructive measurement, polarization filter

Check for updates

OPEN ACCESS

Citation: Faqeerzada MA, Rahman A, Kim G, Park E, Joshi R, Lohumi S, Cho BK. 2020. Prediction of moisture contents in green peppers using hyperspectral imaging based on a polarized lighting system. Korean Journal of Agricultural Science 47:995-1010. https://doi.org/10.7744/kjoas.20200083

Received: August 25, 2020

Revised: October 16, 2020

Accepted: November 17, 2020

Introduction

Pepper (*Capsicum annuum. L*) has its origins in South America at least 9500 years ago (Saxena et al., 2016). Pepper fruits can be used in its premature, ripe, dried, or powdered form (Qin and Lu, 2008, Basak et al., 2019). In all over the world, pepper is one of the most widely consumed produce as spice and seasoning. Thus, a lot of technologies and methods for evaluating its quality and safety have been developed and drawn substantial attentions. As the main component for assessing the quality of produce, measuring the amount of moisture content (MC) has been widely used because the MC decreases after harvested (with an increase of time). Therefore, the determination of the moisture content after harvest using fast and real-time measurement methods allows us to estimate the market value for the product, harvest conditions, and shelf life of fruit, and determine how much water should be removed for drying.

To accomplish this, hyperspectral imaging (HIS) was used in this study because it has been intensively used in agricultural non-destructive applications for evaluating food quality and safety as well as has a high potential for rapid and precise detection of chemical components based on statistical techniques (Kang et al., 2018; Lohumi et al., 2018; Ning et al., 2018; Rahman et al., 2018a; Faqeerzada et al., 2020a; Joshi et al., 2020; Omari et al., 2020). To perform HIS of agricultural products, their biological, chemical, and physical characteristics should be carefully considered such as wrinkles, bruise, sun-glint, shape, and other factors that can affect the intensity of the reflected light source because it is not easy to standardize their own physical and/or chemical properties differently from industrial materials. Thus, the factor which can directly affect the outcome of HSI for evaluating the pepper MC as following.

Green peppers continue to ripen after picking postharvest, thereby causing losses in weight, color, and moisture content, and the appearance of wrinkles at the surface in a short period. Besides, its surface produces natural wax, which appears as powdery bloom to the naked eye, and shows crystalline shape under high magnification. The crystalline shape is different for different fruits, and it gives a shiny surface to fruits. Some fruits have shinier surfaces than others; however, this is not because of the amount of crystalline in the surface of the fruits; rather, it depends on the shape of the skin of a fruit (Kolattukudy, 1984).

Accordingly, the main challenge of HSI is the illumination system set up to handle specular reduction from the surface of samples. The phenomenon of reflecting light from the surface of fruits can be solved by various techniques by having a proper illumination system for capturing the desired image for image analysis. In HSI, the obtained spectral image must be representative of each pixel of the sample.

Therefore, the material must be illuminated equally without the appearances of any shadow or scatter at the surface of the fruits. Many factors cause the glossy surface in the products; some of these are the refractive index of the material surface, angle of the incident light, and topography of the surface (Silvennoinen et al., 2008). For this purpose, to remove the reflection from the surface of products many techniques used computational wise and instrumental uses. Painting and masking are commonly used techniques for removing specular reflection in HSI.

For instance, for detecting a chilling injury in green Jujubes, images were captured using a hyperspectral camera in the reflectance mode, showing that Jujubes with smooth skin scattered light on the surface of the samples. The specular region was painted in each sample before obtaining the mean spectra of each sample. The specular position in each sample was detected from the spectral image in the 680-nm range by creating a mask with a selected threshold value, and the Criminisi algorithm was used to repair the lost region (Lu, 2018). In another study for the detection of bitter pit in storage, HSI was used for imaging apples, and the imaged samples reflected light from the surface, and each sample was used to eliminate the

reflection spots. The saturated spot on the surface of the apple was 3 - 12 times higher than that of the apple tissue, depending on the wavelength. This characteristic for defining a threshold range larger than or equal to three times the reflectance indicated a spectral image, and the resulting image was used to mask the hyperspectral image (Jarolmasjed et al., 2018). The other technique for glare reduction is recommended in a study for early apple bruise detection using HSI. The mean spectra of bruised, unbruised, and glare parts of the sample were compared. The results showed significant differences between the reflectance values of the glaring part and other regions of the apple samples. Owing to spectral non-uniformity, the average spectra of the sample was considered without separating the glossy and sound part (Keresztes et al., 2016).

For uniform illumination, cross-polarization is recommended for glare reduction during fruit inspection based on the measurement of the bidirectional reflectance distribution, shape, and Stokes parameters. For the measured values, a bidirectional reflectance distribution function model is loaded into raytracing to determine the most suitable illumination scheme. This concept was implemented on apples through cross-polarization (CP) with a freeform optic (FO) configuration, which allowed the FO to be optimized to the maximum uniformity by polarizing the parallel gloss and providing 92% light uniformity to prevent reflection (Keresztes et al., 2015).

The commonly used technique for reflection reduction in curve agriculture products is the usage of the dome with a highly reflective coating. For instance, in a study for non-destructive estimation of moisture content, pH, and soluble solids content in tomatoes, HSI system was used in combination with a dome to prevent the reflection of light (Rahman et al., 2017). The outcome of this study is excellent for the prediction of chemical compositions in tomatoes. However, the general disadvantage of the dome is that it creates shadows and needs adjustment for homogenous illuminations. The used techniques of masking and painting of reflected regions in the sample lead to a loss of information from the repaired part. The painted samples losing the usage for mapping the chemical visualization do not reflect the exact information based on the pixels in each region.

The instrumentation techniques, such as CP, used for glare reduction are useful; however, their combination of complex and multiple techniques remove polarizing lighting in the systems. The shiny non-homogenous surface of agricultural products is a major challenge for capturing images without having specular reflection on the surface of the samples. To the best of our knowledge, there is no study on the usage of visible near-infrared hyperspectral imaging (VIS/NIR-HIS) with a polarized lighting system for capturing zero specular reflection on the surface of samples to predict the moisture content in green peppers.

Therefore, the purpose of this study is to use HSI with the polarization of a direct lighting system for the rapid measurement of agricultural products, with the ability to reduce the scatter from the glossy surface of agricultural products with zero reflection. Owing to the glossy surface of green pepper with non-homogenous shape, it was imaged with no scatter from the surface. The specific objectives of this study were (1) polarization of the direct lighting system in the HSI system; (2) extraction of the total spectra of the sample with no specular reflection on the surface of fruits; (3) comparison of extracted spectra of samples with polarized lighting system and non-polarized lighting selected from the region of interest (ROI) of selected samples; (4) development of a model with extracted spectral data for moisture content using the partial least squares (PLS) algorithm with different preprocessing techniques; (5) mapping the chemical image for visualizing the spatial distribution of the moisture content in the samples selected for comparison of spectra from the ROI.

Material and Methods

Green pepper selection

Green pepper was purchased from the local markets in South Korea, which includes three popular varieties: *Nok-Gwang*, *Chug-Yang*, and *Oh-Y-Mat*, and stored at 18℃ overnight before using for measurement. The manually selected samples were of the same size, mature, and free of surface damage. After separating the unwanted sizes, the samples were numbered and weighed them using a digital machine to obtain accurate measurements. The normal weight was found to be 7.8 g, and the length to be 108 mm on the major axis, with an average diameter of 12.55 mm on the minor axis. All selected samples were individually imaged using the HSI system and subsequently used to measure the compositions for reference values.

Hyperspectral imaging system

The samples were imaged using the VIS/NIR-HSI system built by the nondestructive bio-sensing laboratory of Chungnam National University, Daejeon, Republic of Korea. The entire image acquired under the system comprised a line scan imaging spectrograph (Headwall Photonics, Fitchburg, MA, USA), an electron multiplying charge-coupled device (EMCCD) camera of 1,004 (spatial) × 1,002 (spectral) pixels, and a lens with a focal length of 28 mm, f/1.4. The spectral range of the spectrograph covers 400 - 1,000 nm, with a spectral resolution of 7.5 nm, and Fig. 1 is the schematic representation of the HSI system.

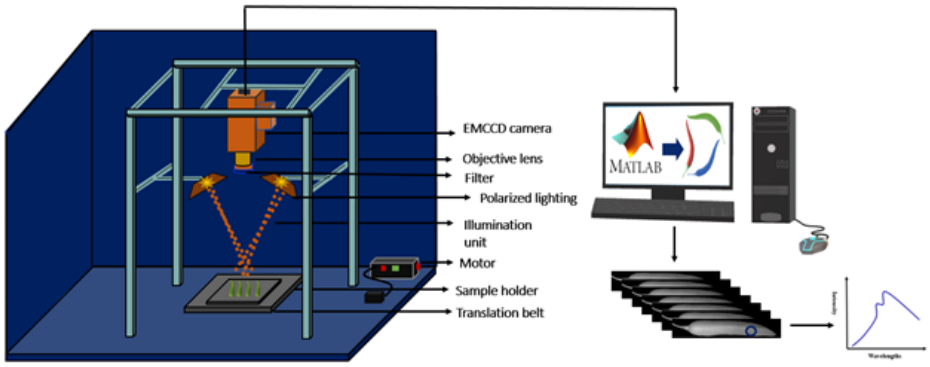

Fig. 1. Hyperspectral imaging system with a polarized lighting system. EMCCD, electron multiplying charge-coupled device.

Direct light system with polarization filter

Specular reflection was produced using the direct lighting system for the glossy surface samples such as the green pepper images. Specular reflection, typically with reflectance values approaching or exceeding 100%, produces highly invalid spectral responses (Park and Lu, 2015). Hence, it is not recommended to use the specular pixels in the dataset for any spectral processing. Therefore, regardless of the source of specular reflection, any pixels with reflectance values close to saturation should be considered with caution.

Specular reflection is often caused by wet or glossy surface features on the sample surface and reflects more when the angle between the incident light and the camera is small or too much of the light is incident on the surface. Meanwhile, the development of the obtained image for the further process relies on how the image is captured using the system. To overcome these challenges, using the polarized lighting system is an excellent solution to capture an image with no specular reflection from the sample surface. As unpolarized light is a complex mixture of random waves and vibrations in a line, wherein linear polarizing selectively absorbs light vibration in certain planes. When light passes through a linear polarizer, its vibrations are confined to a single linear plane. It is possible to transform unpolarized light into polarized light through a process called polarization. The polarization (PL) filter works with the same procedure for blocking unwanted light waves. Based on this principle, a polarizing sheet was installed at the front of light sources and polarizing filters over the camera lens perpendicular to the axis of the polarization linear sheet for maximum glare reduction. Hence, while the generated electromagnetic waves travel from the light sources, they passing through the filter sheet at the front of light sources for illuminating the sample. This light reflects and is polarized by the PL filter at the front of the camera lens. The following procedure was used to capture images with a HSI system. Therefore, the polarized lighting system hyperspectral image was used to image the samples with the following specifications of the filters used at the front of the camera lens and an illumination unit.

In this study, a PL filter sheet was used at the front of a tungsten-halogen (12 V, 100 W, Light Bank, Ushio INC., Tokyo, Japan) direct lighting system for removing specular reflection from the sample surface with a specification of PS 1000, VIS + NIR polarizer film, 400 - 1,000 nm, contrast ratio 5,000 : 1, and temperature range - 20℃ to 60℃. To polarize the reflected light back from the surface of the sample, a glass filter was installed at the front of the camera lens with specification of PR1000-49 (for the lens) VIS + NIR polarizer film, 400 to 1,000 nm, contrast ratio 5,000 : 1, temperature range: - 20℃ to 60℃, and M49 mount.

Image acquisition and spectral data extraction

A sample holder, a stepper motor connected to the PC, and a linear slider were connected to move samples by 0.2 mm under the line scan imaging system. Within an exposure time of 50 ms, the sample was set at a distance of 26 cm from the camera to acquire a complete, clear, and undistorted image. Each scan was run, and the samples were manually loaded onto the sample holder to prevent the shaking and movement of the sample on the table while capturing the image. The acquired image was saved in a three-dimensional (3D) format containing both spectral and spatial information. The custom software of the image acquisition process and system control was developed using Microsoft (MS) Visual Basic (version 6.0, Microsoft, Redmond, USA) and run by the MS Windows system.

To transform the raw hyperspectral images to a reflectance image used, Equation (1) was used to remove the generated noise from the device and the unwanted light intensity, thereby correcting non-uniform light along with the images and producing an image using an actual reflectance scale. The white reference was measured using a white Teflon tile with ≥ 99% reflectance before sample imaging of the sample with the same illumination configuration. The same standard was obtained for the dark (covered lens) references (ca. 0% reflectance) data with the light sources turned off. The calibration image X_{cal} was calculated using the raw hyperspectral image $X_{raw,}$ white reference image $X_{ref,}$ and dark reference image X_{dark} by the equation.

$$X_{cal} = \frac{X_{raw} - X_{dark}}{X_{ref} - X_{dark}} \quad (1)$$

The calibrated hyperspectral image was segmented from the background using the average value of the background and green pepper pixels to remove non-uniform illumination or variation in the pixel-wise sensitivity of the background and fair reflection off the sample (Seo et al., 2019). The dead pixels generated by the camera detector were removed by applying a filter for individual samples. The full spectra were extracted from each sample and averaged before further analysis. A total of 190 spectra extracted from the samples were used for moisture content measurement. All processes were performed using MATLAB (version 8, Math Works Inc., Natick, MA, USA).

Moisture content measurement

Afterimage acquisition, the MC of green pepper was measured via the gravimetric method using oven drying (HST-502M, Hanbaek Co., Ltd., Gwangju, Korea) at 105℃ for 24 h. The weight was measured using an analytical balance (EK-1200i, A&D Company, Tokyo, Japan). For weight measurement, we used Equation (2), as given below. The water content in agricultural material and food products is measured using wet basis moisture. Generally, the sample was dried in an oven and heated to allow for the release of moisture. The sample was cooled before weighing. Moisture content was calculated by the difference in wet and dry weights. In this process, measuring the accuracy and resolution of the balance is extremely important. Careful consideration must also be given to maintaining an identical condition, where temperature and duration are vital for generating precise and reproducible results (Arslan and Özcan, 2011). Equation (2) was used for moisture content calculation considering the initial and final weight.

$$MC_{wb} = \frac{W_i - W_f}{W_i} \times 100 \quad (2)$$

The wet basis moisture content can range from 0 to 100% according to the equation, where the MC_{wb} indicates the moisture content wet basis (%), W_i refers to the initial measured weight, and W_f is the measured final weight after the drying process.

Data analysis

Spectra preprocessing

The objective of the preprocessing of spectral data is to remove phenomena in the spectra in order to improve subsequent multivariate regression. The general use of spectral preprocessing is to correct random noise in spectra, length variation of the light direction and generated light scattering by instruments. Therefore, preprocessing of the obtained data by appropriate mathematical analysis is important to enhance crucial information from the sample and remove unwanted variations from the spectral data. Therefore, to obtain smooth images without artifact variations and physical causes needed to preprocess, spectral data must be processed (Rinnan et al., 2009). In this study, normalization, smoothing, multiplicative scatter correction (MSC), standard normal variate (SNV), and Savitzky–Golay first and second derivative preprocessing methods were used to eliminate noise and undesired elements from the spectral data (Kandpal et al., 2013; Rahman et al., 2018b; Wakholi et al., 2018; Joshi et al., 2019; Faqeerzada et al, 2020b).

Development of calibration model

Outlier detection is an important process in the multivariate calibration of data. Through this process, we can determine the quality of the calibration dataset and a calibration model. According to different studies, outliers in multivariate analysis of the calibration dataset is a serious challenge because it has a significant effect on the quality model (Liang and Kvalheim, 1996). In another study, the existence of a single outlier data in the calibration set had a significantly larger and detrimental effect on the model than normal samples, leading to a complex statistical calculation with different results (Møller et al., 2005). The outlier was removed using the procedure introduced by Valderrama et al. (2007) owing to the existence of residual independent variables ($Y_{residual} = Y_{predicted} - Y\ m_{easured)}$. Outliers are detected by comparing the root-mean-square error of calibration with the absolute error of that sample. The most common cause of outliers in data is laboratory error objects from another population, instrument error (Martens and Naes, 1989).

After outlier detection and preprocessing of the spectra, the samples were divided into two sets—calibration and prediction. Hence, from the total of 190 expected samples, 186 samples were used for moisture content: the calibration set comprised 126 samples and the prediction set comprised 60 samples; the remaining samples were removed as they were detected as outliers.

In this study, partial least squares regression (PLSR) multivariate analysis was used to improve a calibration model for green pepper chemical composition prediction. PLSR is a multivariate analysis technique that generalizes and combines features from principal component analysis and multiple regression (Rahman et al., 2017). It is widely used as a multivariate calibration method for processing large amounts of data to predict the behavior of dependent variables based on large datasets of independent variables (Kandpal et al., 2013; Lohumi et al., 2018b). The PLSR model depends on the X and Y variables in a designed matrix, in which the linear relation between axes of X and Y enables the model to predict components in the Y variables (Burns and Ciurczak, 2007). The detailed definitions of the model based on mathematics are as follows in Equations (3) and (4).

$$X = TP^{T} + E \tag{3}$$

$$Y = UQ^{T} + E \tag{4}$$

According to the model, X and Y are the independent and dependent variables, respectively, while T and U denote the score matrices. P^{T} and Q^{T} are the X and Y variable loading in matrices, respectively, and E is considered as the error of the matrix. The X-axis indicates the spectral data extracted from green pepper, and the Y-axis represents the measured moisture content. Additionally, the PLSR model builds using the calibration and tests the validation dataset. Developing a model that selects the number of latent variables is important to avoid overfitting and underfitting, which creates noise in regression of the model, spectral signature, and model interpretation. In this study, the number of Latent variables (LVs) selected based on the minimum value of the root-mean-square error by applying Equation (5).

$$\mathrm{RMSE} = \frac{1}{z}\sqrt{\Sigma_{i=1}^{2}(y_i - \hat{y}_i)^2} \tag{5}$$

where y_i is the actual reference value of green pepper, y_i is the value of the predicted parameter from the PLSR, and z is the number of predictions.

Chemical Image

One major advantage of HSI is the ability to create a chemical image of the component distribution from the simultaneous measurement of spectral and spatial data. The novel benefit of the chemical image is the measurement of different parameters of the chemical component sample to sample and with the same sample at each pixel location (Rahman et al., 2017). The PLSR model was used to visualize and map the quality attributes of moisture content in every pixel of HSI, through the selected vital wavelength selection from the beta coefficient curve resulting from the calibration model. The hyperspectral image based on selected wavelengths was advanced into a 2D matrix and multiplied by the PLSR coefficient. The obtained vector was folded back into the 2D image, and this 2D image showed the visualization of different chemical parameters in the green pepper samples. The final chemical images were obtained by applying Equation (6).

$$\text{Chemical Image} = \sum_{i=1}^{n} I_i R_i + C \quad (6)$$

where I_i is the image of a non-reflectance spectral image and R_i is the beta coefficient derived from the PLSR model.

Result and Discussion

Hyperspectral image of green pepper (direct light vs. polarized direct lighting system)

The potential of the PL filter for glare reduction on the surface of fruits can be observed in the image, with the sample being imaged with the polarized and non-polarized lighting system using both RGB imaging camera and a HSI system. Fig. 2a and 2b show that the RGB imaging camera captured an image for observing the light scatter from the surface of the sample. Fig. 2a shows no reflection on the surface of the green peppers and the second image Fig. 2b with non-polarized lighting shows specular reflection at the surface of the samples. The images were captured with the same parameters using HSI, while the figures indicate the image captured with the polarized lighting system Fig. 2c shows glare less at the surface of the sample. The image scanned under the direct lighting system without polarization showed gloss clearly at the surface of the image, as shown in Fig. 2d.

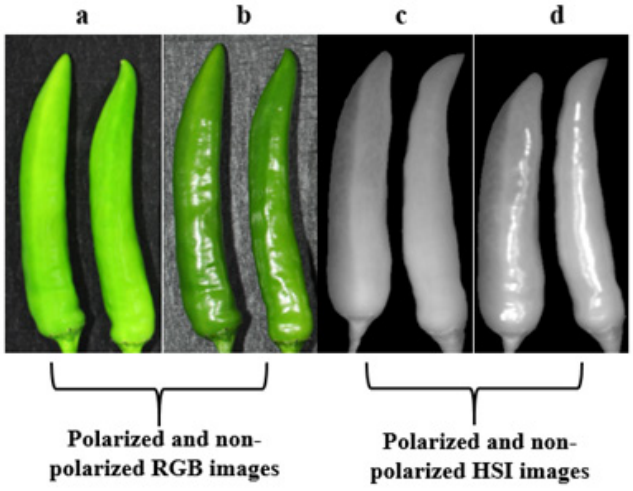

Fig. 2. RGB image (a) with the polarized lighting system and (b) without the polarized lighting system. The hyperspectral image of green pepper (c) with a polarized lighting system and (d) direct lighting without a polarization system. HIS, hyperspectral imaging.

Accordingly, the images without polarized lighting systems clearly show the non-uniform surface of reflected light; therefore, the extracted spectral data might not present the exact chemical composition due to specular reflection. Also, the spectra intensity obtained from non-polarized images will be affected. Then, the spectra of both samples were obtained and Fig. 3 presents the extracted ROI spectral data from the same sample related to glare reflection and non-glare portions showing obvious differences in spectral intensity and patterns.

In Fig. 3, red and blue lines are the specular ROI and non-specular ROI, respectively. As we expected above, specular ROI shows a much higher intensity (about 3 times) than that of non-specular ROI due to the specular effect. Therefore, it is not recommended to use the extracted spectra from the samples with the glossy surface using HSI without a polarized lighting system. As the results show the spectral changes in the same sample, developing a chemical image without a uniform lighting system is challenging.

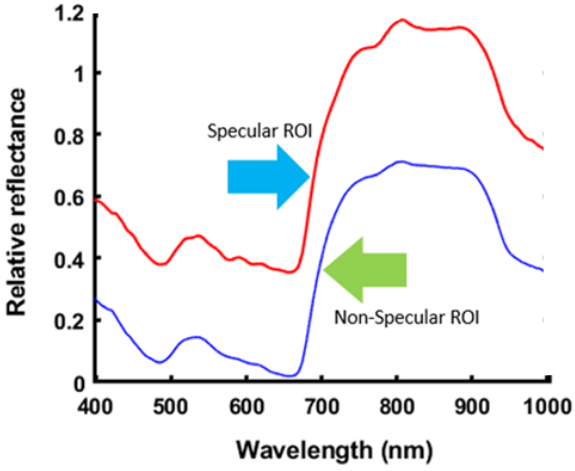

Fig. 3. Mean spectra extracted from hyperspectral images of green pepper samples were collected from the non-glare part (blue) and the glaring part of the sample (red). ROI, region of interest.

Spectral profile of green pepper

Fig. 4 shows the average raw spectra of green peppers in the range of 400 - 1,000 nm, which was used to preprocess the SG-2nd derivative. The near-infrared region was sensitive to the concentration of organic components in the samples, and the most prominent absorption band occurring in the NIR region is related to the overtone and vibration of C-H, N-H, and O-H (Blanco and Villarroya, 2002). Thus, most chemical and biochemical species exhibit a unique absorption band in the NIR spectral region that can be used for both qualitative and quantitative purposes (Metrohm, 2013). There are peaks in the region at 720, 911, and 976 mm, indicating the existence of water in the regions (Zhao et al., 2016).

Table 1 below includes statistical values such as the number of samples, range, mean, and standard deviation (SD) of the measured moisture content using oven drying. According to Table 1, the samples were divided into two sets calibration and prediction of the number of samples considering 130 samples in the calibration set and 60 samples in the validation set.

In Table 1, to develop a more precise MC model, the outliers were removed from pure data. After removing outliers, 126 samples remained in the calibration set for moisture content, and 4 samples were removed from pure data as outliers.

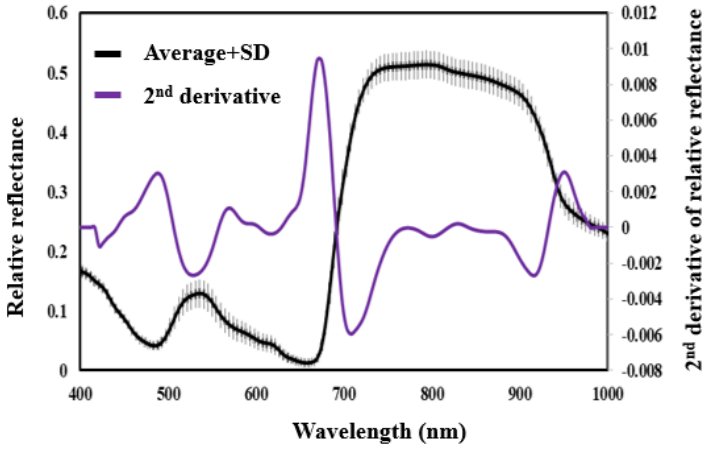

Fig. 4. Average raw spectra and Savitzky–Golay 2nd derivative preprocessed spectra of green pepper.

Table 1. Descriptive statistics of calibration and prediction datasets.

Parameters	Descriptive statistics	No. of sample	Max	Min	Mean ± SD
MC (%)	Calibration	130	92.71	86.91	90.12 ± 1.28
	Prediction	60	92.85	87.25	90.16 ± 1.32

Min, minimum; Max, maximum; SD, standard déviations.

PLSR calibration model results for moisture content

The calibration and predicted results of MC were obtained from the developed model with different preprocessing methods shown in Table 2. Among the calibration models, the MSC preprocessed spectra-based model exhibits better performance. The scatter in Fig. 5 shows a strong correlation between the actual and predicted values of the respective parameter. The calibration correlation between the spectra and moisture content of green pepper was high, with an R^2 value of 0.93, while the model applied to the prediction set resulted in an R^2 value of 0.89 using the MSC preprocessed spectra.

Because the comparison of the developed models to select the best model is important in spectral analysis the developed models can be compared in terms of the performance of the calibration model by using different preprocessing techniques for selecting the top resulted in spectra preprocessing. The determination coefficients of the developed models obtained the full spectra and the developed models compared in Table 2.

Based on Table 2, although the determinant coefficients of the calibration and prediction were about 0.9 from all preprocessing methods and there was no dramatic change, among the spectral preprocessing techniques used for the development model, the MSC-based spectral preprocessing developed model shows the best prediction of green pepper chemical compositions. The developed model for the prediction of moisture content is plotted in Fig. 5. However, the other preprocessed model presented good results. For instance, the developed model with SG-1st derivatives shows the closest result to the MSC with resulted in R^2cal = 0.93, SEC of 0.48%, and R^2pre = 0.89 for moisture content. According to the plots that show the calibration and predicted the results for moisture content, the y-axis represents the values of measured parameters, and the x-axis represents the predicted values for each parameter considered for analysis.

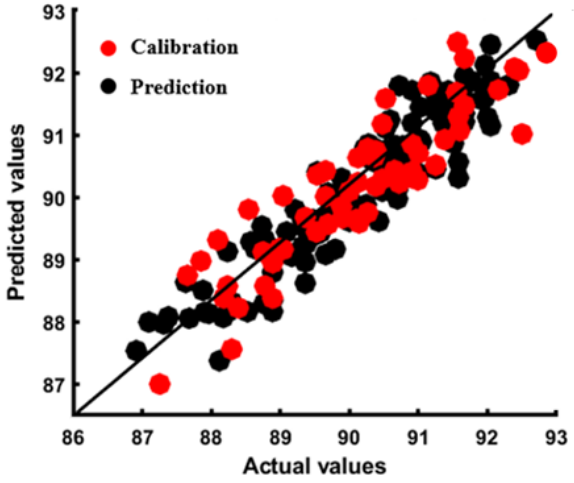

Fig. 5. Regression plot for moisture content obtained from the PLSR model developed with MSC preprocessed data. PLSR, partial least square regression; MSC, multiplicative scatter correction.

Table 2. PLSR analysis results were obtained for the prediction of moisture content in green pepper samples.

Preprocessing method	Moisture montent			
	R^2_{cal}	SEC (%)	R^2_{pre}	SEP (%)
Original	0.93	0.45	0.90	0.57
Smoothing	0.92	0.49	0.89	0.59
Max normalization	0.92	0.47	0.89	0.59
Mean normalization	0.93	0.46	0.90	0.56
Range normalization	0.92	0.48	0.91	0.55
MSC	0.93	0.46	0.89	0.58
SNV	0.92	0.49	0.89	0.58
SG 1st derivatives	0.92	0.48	0.89	0.58
SG 2nd derivatives	0.92	0.45	0.88	0.61

PLSR, partial least square regression; R^2_{cal}, determination of coefficient for calibration; SEC, standard error of calibration; R^2_{pre}, determination of coefficient for prediction; SEP, standard error of prediction; MSC, multiplicative scatter correction; SNV, standard normal variate; SG, Savitzky-Golay.

The analytical ability of visible near-infrared depends on the repetitive and broad absorption of light by C-H, O-H, and N-H bonds (Xuemei and Jianshe, 2013). In this study, the beta coefficient resultant from the PLS beta coefficient curve in the range of 400 - 1,000 nm was used to develop a chemical composition distribution in the green peppers. Fig. 6 depicted high absorption peaks presented in the 900 nm and 970 nm bands related to the water (Clevers et al., 2008; Seelig et al., 2008), which are the significant bands for the moisture content prediction of green peppers. As well in other studies, the 970 nm peak was indicated as the most significant peak for water content absorption (Penuelas et al., 1993; Jiao et al., 2020). However, there are many high peak wavelengths, for instance around 510 nm, 550, and 650 nm, and the high peaks indicate chlorophyll stretch bands (Zhao et al., 2016) where green pepper comprise high chlorophytes. The selected bands are marked in the plots indicating the existence of chemical compositions and groups in the green peppers.

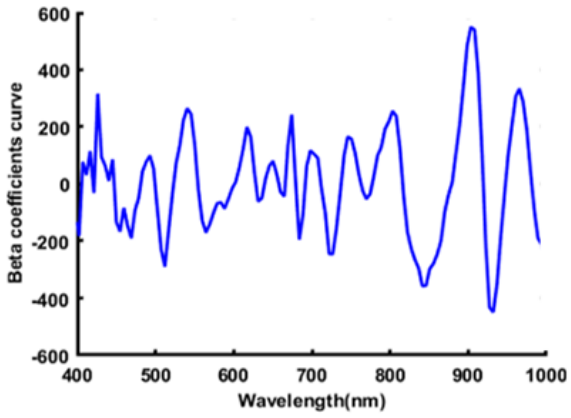

Fig. 6. Beta coefficient curve from the partial least square regression (PLSR) model developed for moisture content.

Visualization of moisture content in green pepper

A major benefit of HSI is that it measures the particular chemical components in a specific location, and it is advantageous for the identification and quantification of chemical components in a sample (Kandpal et al., 2013). In this study, the beta coefficient (correlation coefficient) value obtained from the best-preprocessed spectra was used to create the moisture content chemical image and then multiplied with the spectrum of each pixel of the original hyperspectral image of the green pepper sample.

In addition, the samples used for the development of the chemical image in Fig. 7, according to appearance observation of the samples and the color bar with the intensity from (60 - 100) show that the moisture content with polarized lighting system samples has the moisture content with uniform distribution. Furthermore, the image with a non-polarized lighting system shows the reflection with dark red color and non-uniform distribution of the moisture content in the sample.

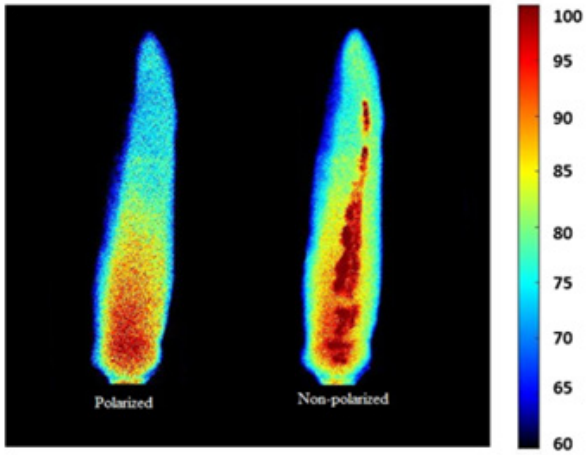

Fig. 7. Partial least square regression (PLSR)-based chemical image for moisture content of green pepper scanned with and without customized polarization.

In Fig. 7, the mesocarp is located in the center of the pepper and holds most of the absorbed water while also providing structural support for the pepper, and the endocarp is the membrane layer surrounding the seeds of the pepper that absorbs the water. Fig. 8 presents the cut green pepper for moisture content distribution, the color bar with the intensity from (60 - 100) shows that the central part and seeds are the most concentrated water part in the green peppers.

Finally, the highest concentration of the moisture is found closer to the seeds of the pepper. The figure indicates the distribution of moisture contents in cut green peppers and presents the chemical compositions based on the color bar, which goes from dark blue to dark red, and the middle of the peppers due to the high concentration of water in the placenta and absorbed by the seeds showed a red dark concentrated area.

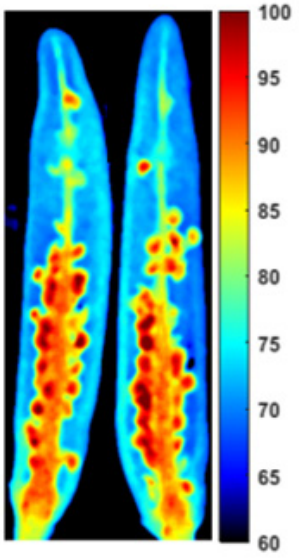

Fig. 8. Moisture content distribution in cut green pepper.

Conclusion

In this study, polarized and non-polarized direct lighting with the VIS-NIR HSI system was used to predict the moisture content of green pepper. Initially, the HSI image of green pepper was inspected and captured using the polarized and non-polarized direct lighting systems. The results showed that there is a high potential of a polarized direct lighting system for gloss reduction from the shiny surface of green pepper, for accurate and correct HSI images for further prediction analysis. In contrast, the non-polarized direct lighting system HSI image showed that the surface of the sample had higher intensity due to light scattering. Subsequently, the PLSR model was developed using different preprocessed spectra extracted from the polarized directing lighting system HSI green pepper image. The results demonstrated a determination coefficient (R^2_{pre}) of 0.89 for moisture content with MSC preprocessing. The regression coefficients yielded by the best PLSR model were used to select the important wavelengths for creating the mapping image of the chemical components. Thus, the polarizing direct lighting system helps improve the quality of hyperspectral images via the reduction of gloss, thereby presenting highly accurate statistical data and predicting the moisture content in green peppers.

Acknowledgment

This work was supported by the research fund of Chungnam National University.

Authors Information

Mohammad Akbar Faqeerzada, https://orcid.org/0000-0002-1829-2502

Anisur Rahman, https://orcid.org/0000-0003-1466-4310

Geonwoo Kim, https://orcid.org/0000-0002-6274-3649

Eunsoo Park, https://orcid.org/0000-0002-5834-2893

Rahul Joshi, https://orcid.org/0000-0003-1466-4310

Santosh Lohumi, https://orcid.org/0000-0002-5437-2411

Byoung-Kwan Cho, https://orcid.org/0000-0002-8397-9853

References

Arslan D, Özcan MM. 2011. Dehydration of red bell-pepper (*Capsicum annuum* L.): Change in drying behavior, colour and antioxidant content. Journal of Food and Bioproducts Processing 89:504-513.

Basak JK, Qasim W, Okyere FG, Khan F, Lee YJ, Park J, Kim HT. 2019. Regression analysis to estimate morphology parameters of pepper plant in a controlled greenhouse system. Journal of Biosystem Engineering 44:57-68.

Blanco M, Villarroya I. 2002. NIR spectroscopy: A rapid-response analytical tool. Journal of Trends Analytical Chemistry 21:240-250.

Burns DA, Ciurczak EW. 2007. Handbook of near-infrared analysis. *II (3rd)* edited by Taylor and Francis. pp. 189-205. Published Group, New York, USA.

Clevers JGPW, Kooistra L, Schaepman ME. 2008. Using spectral information from the NIR water absorption for the retrieval of canopy water content. International Journal of Earth Observation and Geoinformation 10:388-397.

Faqeerzada MA, Lohumi S, Kim G, Joshi R, Lee H, Kim SM, Cho BK. 2020b. Hyperspectral shortwave infrared image analysis for detection of adulterants in almond powder with one-class classification method. Journal of Sensors 20:5855.

Faqeerzada MA, Parez M, Lohumi S, Lee H, Kim G, Wakholi C, Joshi R, Cho BK. 2020a. Online application of a hyperspectral imaging system for the sorting of adulterated almonds. Journal of Applied Science 10:6569.

Jarolmasjed S, Khot LR, Sankaran S. 2018. Hyperspectral imaging and spectrometry-derived spectral features for bitter pit detection in storage apples. Journal of Sensors 18:1561.

Jiao Q, Liu L, Liu J, Zhang H, Zhang B. 2020. Atmospherically resistant vegetation water indices using the 970-nm water absorption feature. Journal of Applied Remote Sensing 14:1-21.

Joshi R, Cho BK, Lohumi S, Joshi R, Lee J, Lee H, Mo C. 2019. Evaluation of benzene residue in edible oils using Fourier transform infrared (FTIR) spectroscopy. Korean Journal of Agricultural Science 46:257-271.

Joshi R, Lohumi S, Joshi R, Kim MS, Qin J, Baek I, Cho BK. 2020. Raman spectral analysis for non-invasive detection of external and internal parameters of fake eggs. Journal of Sensors and Actuators B: Chemical 303:127243.

Kandpal L, Lee H, Kim M, Mo C, Cho BK. 2013. Hyperspectral reflectance imaging technique for visualization of moisture distribution in cooked chicken breast. Journal of Sensors 13:13289-13300.

Kang YS, Ryu SC, Kim SH, Jun SR, Jang SH, Park JW, Song H. 2018. Yield prediction of Chinses cabbage (Brassicaceae) using broadband multispectral imagery mounted unmanned aerial system in the air and narrowband hyperspectral imagery on the ground. Journal of Biosystems Engineering 43:138-147.

Keresztes JC, Goodarzi M, Saeys W. 2016. Real-time pixel based early apple bruise detection using short wave infrared hyperspectral imaging in combination with calibration and glare correction techniques. Journal of Food Control 66:215-226.

Keresztes JC, Koshel RJ, Chipman R, Stover JC, Saeys W. 2015. A cross-polarized freeform illumination design for glare reduction in fruit quality inspection. Proceedings of SPIE is the conference record of the Society of Photo-Optical Instrumentation Engineers 219:38-58.

Kolattukudy PE. 1984. Natural waxes on fruits. Postharvest Information Network 2:1-4.

Liang YZ, Kvalheim OM. 1996. Robust methods for multivariate analysis: A tutorial review. Chemometrics and Intelligent Laboratory Systems 32:1-10.

Lohumi S, Lee H, Kim MS, Qin J, Cho BK. 2018. Through-packaging analysis of butter adulteration using line-scan spatially offset Raman spectroscopy. Analytical and Bioanalytical Chemistry 410:5663-5673.

Lu H. 2018. Selection of spectral resolution and scanning speed for detecting green jujubes chilling injury based on hyperspectral reflectance imaging. Journal of Applied Sciences 8:1-13.

Martens H, Naes T. 1989. Multi variate calibration. pp. 164-168. Editied by John. Wiley, New York, USA.

Metrohm. 2013. NIR Spectroscopy: A guide to near-infrared spectroscopic analysis of industrial manufacturing processes. Printed in Switzerland by Metrohm AG. CH-9101, Herisau, Switzerland.

Møller SF, Frese JV, Bro R. 2005. Robust methods for multivariate data analysis. Journal of Chemometrics 19:549-563.

Ning XF, Gong YJ, Chen YL, Li H. 2018. Construction of a ginsenoside content predicting model based on hyperspectral imaging. Journal of Biosystem Engineering 43:369-378.

Omari MK, Lee J, Faqeerzada MA, Joshi R, Park E, Cho BK. 2020. Digital image-based plant phenotyping: A review. Korean Journal of Agricultural Science 47:119-130.

Park B, Lu R. 2015. Hyperspectral imaging technology in food and agriculture. I (1st) Gustavo V. Barbosa-Ca´novas. pp. 86-110. Publisher Springer-Verlag, New York, USA.

Penuelas J, Filella I, Biel C, Serrano L, Save R. 1993. The reflectance at 950-970 nm region as an indicato of plant water status. International Journal of Remote Sensing 10:1887-1905.

Qin J, Lu R. 2008. Measurement of the optical properties of fruits and vegetables using spatially resolved hyperspectral diffuse reflectance imaging technique. Journal of Postharvest Biology and Technology 49:355-365.

Rahman A, Faqeerzada MA, Joshi R, Lohumi S, Kandpal LM, Lee H, Mo C, Kim MS, Cho BK. 2018a. Quality analysis of stored bell peppers using near infrared hyperspectral imaging. Journal of American Society of Agriculture and Biology Engineering 61:1199-1207.

Rahman A, Kandpal LM, Lohumi S, Kim MS, Lee H, Mo C, Cho BK. 2017. Nondestructive estimation of moisture content, pH and soluble solid contents in intact tomatoes using hyperspectral imaging. Journal of Applied Science 7:109.

Rahman A, Lee H, Kim MS, Cho BK. 2018b. Mapping the pungency of green pepper using hyperspectral imaging. Journal of Food Analytical Methods 11:3042-3052.

Rinnan Å, Berg FVD, Engelsen SB. 2009. Review of the most common pre-processing techniques for near-infrared spectra. Journal of Trends in Analytical Chemistry 28:1201-1222.

Saxena A, Raghuwanshi R, Gupta VK, Singh HB. 2016. Chilli anthracnose: The epidemiology and management. Frontiers in Microbiolgy 7:1-18.

Seelig HD, Hoehn A, Stodieck LS, Klaus D, Adams WW, Emery WJ. 2008. The assessement of leaf water content reflectance ratios in the visible, near, and short-wave-inferared. International Journal of Remote sensing 29:3701-3713.

Seo Y, Lee H, Bae HJ, Park E, Lim HS, Kim MS, Cho BK. 2019. Optimized multivariate analysis for the discrimination of cucumber green mosaic mottle virus-infected watermelon seeds based on spectral imaging. Journal of Biosystem Engineering 44:95-102.

Silvennoinen R, Peiponen KE, Myller K. 2008. Specular Gloss. I (1st). pp.83-101. Elsevier Ltd., Great Britain, UK.

Valderrama P, Willian JB, Braga JWB, Poppi RJ. 2007. Study for the determination of quality parameters in a partial least-squares regression multivariate calibration model. A case study for the determination of quality parameters

in the alcohol industry by near-infrared spectroscopy. Journal of Agricultural and Food Chemiestry 55:8331-8338.
Wakholi C, Kandpal LM, Lee H, Bae H, Park E, Kim MS, Mo C, Lee WH, Cho BK. 2018. Rapid assessment of corn seed viability using short wave infrared line-scan hyperspectral imaging and chemometrics. Journal of Sensors and Actuators B: Chemical 255:498-507.
Xuemei L, Jianshe L. 2013. Measurement of soil properties using visible and short wave-near infrared spectroscopy and multivariate calibration. Journal of Measurement 46:3808-3814.
Zhao YR, Li X, Yu KQ, Cheng F, He Y. 2016. Hyperspectral Imaging for determining pigment contents in cucumber leaves in response to angular leaf spot disease. Journal of Scientific Report Nature 6:1-9.